Mon. Not. R. Astron. Soc. **369,** 1797–1807 (2006) doi:10.1111/j.1365-2966.2006.10417.x

Neutron-loaded outflows in gamma-ray bursts

Elena M. Rossi,[1,2⋆] Andrei M. Beloborodov[3,4⋆] and Martin J. Rees[1⋆]

[1]*Institute of Astronomy, University of Cambridge, Madingley Road, Cambridge CB3 0HA*
[2]*Max Planck Institute for Astrophysics, Garching, Karl-Schwarzschild-Str. 1, D-85741 Garching, Germany*
[3]*Physics Department and Columbia Astrophysics Laboratory, Columbia University, 538 W 120th Street, New York, NY 10027, USA*
[4]*Astro-Space Center of Lebedev Physical Institute, Profsojuznaja 84/32, Moscow 117810, Russia*

Accepted 2006 April 4. Received 2006 April 4; in original form 2005 December 20

ABSTRACT

Relativistic neutron-loaded outflows in gamma-ray bursts are studied at their early stages, before deceleration by a surrounding medium. The outflow has four components: radiation, electrons, protons and neutrons. The components interact with each other and exchange energy as the outflow expands. The presence of neutrons significantly changes the outflow evolution. Before neutrons decouple from protons, friction between the two components increases their temperatures by many orders of magnitude. After the decoupling, the gradual neutron decay inside the outflow has a drag effect on the protons and reduces their final Lorentz factor. In inhomogenous outflows, this drag can reduce the Lorentz-factor contrast and affect the development and strength of internal shocks.

Key words: hydrodynamics – relativity – gamma-rays: bursts.

1 INTRODUCTION

A neutron component in gamma-ray bursts (GRBs) was proposed by Derishev, Kocharovsky & Kocharovsky (1999a,b), and detailed calculations of nuclear composition show that free neutrons are inevitably present among ejected baryons (Beloborodov 2003b, hereafter B03b). Any plausible central engine of GRBs is dense and at least mildly degenerate, which leads to its neutronization. During the explosion, the expanding neutron-rich material may undergo nucleosynthesis: neutrons tend to recombine with protons to α particles (Lemoine 2002; Pruet, Guiles & Fuller 2002; B03b). This recombination may be successful if the outflow is collimated. However, even in an extreme case of a very efficient recombination, a significant neutron component is left over in neutron-rich outflows because the formation of α particles consumes equal numbers of neutrons and protons. The abundance of leftover neutrons may vary from 10 to more than 90 per cent depending on the precise parameters of the burst.

The presence of neutrons changes the theoretical picture of GRB explosion. First, they may develop a somewhat smaller Lorentz factor than protons. When such a decoupling takes place, the last n–p collisions lead to emission of observable multi-GeV neutrinos (Derishev et al. 1999a, hereafter DKK99a; Bahcall & Mészáros 2000; Mészáros & Rees 2000a). Secondly, neutrons decay with time. The decay impacts the external blast wave at radii $r \sim 10^{16}$–10^{17} cm because even an exponentially small number of survived neutrons carry an energy much larger than the rest energy of external medium (Beloborodov 2003a).

In the present paper, we study the dynamics of neutron-loaded outflows at early stages of their expansion, $r < 10^{16}$ cm, before they are decelerated by an external medium. The neutrons decay gradually at all radii $r \lesssim 10^{17}$ cm, and at small r the decay occurs *inside* the GRB outflow. The decay turns out important at r as small as 10^{12} cm.

Interesting effects also take place at small $r < 10^{12}$ cm. Neutrons are initially accelerated together with protons because they are collisionally coupled, and the last n–p collisions before decoupling cause a significant heating.

We assume in this paper a simple hydrodynamic picture of expansion driven by thermal pressure and study the basic dynamics of a uniform neutron-loaded outflow. We do not consider internal shocks or possible dynamical effects of magnetic fields. The paper is organized as follows. In Section 2, we briefly review neutron-free outflows, which have been studied previously in detail (see Piran 1999, for a review). In Section 3, we derive equations describing neutron-loaded outflows and calculate example numerical models. Results are discussed in Section 4.

2 NEUTRON-FREE OUTFLOW

We model the GRB outflow as a steady wind with duration $t_{\rm GRB}$, luminosity L and baryon mass outflow rate $\dot{M}$. We assume spherical symmetry. This is a good approximation also for jets with constant opening angle greater than $1/\Gamma$ – such a jet behaves as a part of a spherically symmetric outflow. The main parameter of

⋆E-mail: emr@jilau1.colorado.edu (EMR); amb@phys.columbia.edu (AMB); mjr@ast.cam.ac.uk (MJR)

the problem is

$$\eta = \frac{L}{\dot{M}\,c^2} \sim 10^2\text{–}10^3. \tag{1}$$

We consider three components in this section: radiation, electrons and protons. The plasma is injected into a region of size R_0. At small radii $r \lesssim 30R_0$, the outflow is dominated by $e^{\pm}$ pairs, all components maintain a common temperature and cool adiabatically. An interesting evolution begins at $r > 50\,R_0$ where $e^{\pm}$ can be neglected.

2.1 Opaque stage

2.1.1 Outflow acceleration

As long as the outflow is optically thick, electrons, protons and radiation behave as a single relativistic fluid. The fluid has four-velocity $U^\alpha = (\Gamma_{\rm p}c,\, \Gamma_{\rm p}\beta_{\rm p}c,\, 0,\, 0)$ in spherical coordinates $(t,\, r,\, \theta,\, \phi)$. The trapped radiation is isotropic in the fluid frame and described by the blackbody law with a temperature $T_{\rm r}$.

The total stress energy tensor of the fluid is then given by (e.g. Misner, Thorne & Wheeler 1973)

$$\mathcal{T}^{\alpha\beta} = \left(\frac{4}{3}a\,T_{\rm r}^4 + \rho_{\rm p}\,c^2\right)\frac{U^\alpha U^\beta}{c^2} + \frac{1}{3}\,aT_{\rm r}^4 g^{\alpha\beta}, \tag{2}$$

where $a = 7.56 \times 10^{-15}\ {\rm erg\,cm^{-3}}\ K^{-4}$ is the radiation constant and $g^{\alpha\beta} = {\rm diag}\,(-1,\, 1,\, r^2,\, r^2\sin^2\theta)$ is Minkowski metric in coordinates $(t,\, r,\, \theta,\, \phi)$. The plasma contribution to the energy density is taken equal to $\rho_{\rm p}\,c^2$, where $\rho_{\rm p}$ is the proper mass density of protons; small contributions from e and p thermal motions and the electron rest mass are neglected. The four-vector of baryon mass flux is given by

$$F^\alpha = \rho_{\rm p}\,U^\alpha. \tag{3}$$

The outflow dynamics is governed by the conservation laws

$$\frac{\partial \mathcal{T}^{\rm tt}}{\partial t} = -\frac{1}{r^2}\frac{\partial(r^2\,\mathcal{T}^{\rm tr})}{\partial r}, \tag{4}$$

$$\frac{\partial F^{\rm t}}{\partial t} = -\frac{1}{r^2}\frac{\partial(r^2\,F^{\rm r})}{\partial r}. \tag{5}$$

As long as $r < t_{\rm GRB}\,c\,\Gamma_{\rm p}^2$ (which we assume to be satisfied thereafter) the outflow may be described as a steady-state wind, so that $\partial/\partial t = 0$. [1] Then the conservation laws give

$$L = 4\pi r^2 c\beta_{\rm p}\Gamma_{\rm p}^2\left(\frac{4}{3}a\,T_{\rm r}^4 + \rho_{\rm p}\,c^2\right) = {\rm const}, \tag{6}$$

$$\dot{M} = 4\pi r^2 c\beta_{\rm p}\Gamma_{\rm p}\rho_{\rm p} = {\rm const}. \tag{7}$$

The ratio of these two constants is the parameter η (equation 1).

The description of fluid dynamics will be complete once we specify the evolution of radiation temperature $T_{\rm r}$ with radius. The photon-to-baryon ratio in GRB outflows is $\sim 10^5$ (see e.g. equation 68 in B03b) and their internal energy is strongly dominated by radiation. Energy exchange between radiation and plasma practically does not affect $T_{\rm r}$ and it follows the adiabatic law,

$$T_{\rm r} = T_0\left(\frac{n}{n_0}\right)^{1/3}, \tag{8}$$

[1] At radii $r < t_{\rm GRB}\,c\,\Gamma_{\rm p}^2$ the leading and trailing parts of the outflow are causally disconnected. Therefore, the outflow behaves as part of a steady wind despite the fact that geometrically it is a thin shell already at $r > t_{\rm GRB}\,c$.

$$n = n_0\left(\frac{r}{R_0}\right)^{-2}\frac{1}{\Gamma_{\rm p}\beta_{\rm p}}, \tag{9}$$

where $n = \rho_{\rm p}/m_{\rm p}$ is the proton number density; T_0 and n_0 are constants defined at the base of the outflow $r = R_0 \sim 10^6$–10^7 cm,

$$T_0 \equiv \left(\frac{3\,L}{16\pi\Gamma_0^2\beta_0\,R_0^2\,c\,a}\right)^{1/4} \approx 10^{10}\,\frac{L_{52}^{1/4}}{R_{07}^{1/2}}\ {\rm K}, \tag{10}$$

$$n_0 \equiv \frac{L}{4\pi\,\Gamma_0\beta_0 R_0^2 m_{\rm p}\,c^3\,\eta} \approx 6\times 10^{26}\frac{L_{52}}{R_{07}^2}\left(\frac{\eta}{300}\right)^{-1}\ {\rm cm^{-3}}, \tag{11}$$

where $\Gamma_0 = \Gamma_{\rm p}(R_0)$ and we assume

$$\Gamma_0\beta_0 = 1. \tag{12}$$

Equations (6)–(8) give a closed description of the outflow dynamics at the opaque stage of its expansion. Combining the equations we find

$$\Gamma_{\rm p}(1+x) = \eta, \tag{13}$$

where

$$x \equiv \frac{4}{3}\frac{aT_{\rm r}^4}{nm_{\rm p}c^2} = x_0\left(\frac{n}{n_0}\right)^{1/3}, \qquad x_0 = \frac{\eta}{\Gamma_0} - 1, \tag{14}$$

and obtain the algebraic equation for $\Gamma_{\rm p}(r)$,

$$\left(\frac{\eta}{\Gamma_{\rm p}} - 1\right)\left(\Gamma_{\rm p}^2 - 1\right)^{1/6} = x_0\left(\frac{r}{R_0}\right)^{-2/3} \tag{15}$$

(see also DKK99a).

2.1.2 Thermal balance

The evolution of electron temperature $T_{\rm e}$ and proton temperature $T_{\rm p}$ in general depends on their energy exchange with each other and radiation. It turns out that all components of the neutron-free outflow maintain the common temperature $T_{\rm e} \approx T_{\rm p} \approx T_{\rm r}$ during the opaque stage. We shall verify this with an accurate thermodynamic calculation.

The electron and proton components obey the first law of thermodynamics,

$${\rm d}U_{\rm i} = {\rm d}Q_{\rm i} + (U_{\rm i} + P_{\rm i})\frac{{\rm d}n}{n}, \qquad {\rm i} = {\rm e},\, {\rm p}, \tag{16}$$

where $U_{\rm i}$ is internal energy density of component i, d $Q_{\rm i}$ is heat received by component i per unit volume and $P_{\rm i}$ is its pressure; all the quantities are measured in the fluid frame. $U_{\rm i}$ and $P_{\rm i}$ are related to temperature $T_{\rm i}$,

$$U_{\rm i} = \frac{nkT_{\rm i}}{\hat{\gamma}_{\rm i} - 1}, \qquad P_{\rm i} = nkT_{\rm i}, \qquad {\rm i} = {\rm e},\, {\rm p}, \tag{17}$$

where $\hat{\gamma}_{\rm i}$ is the adiabatic index of component i; it equals 5/3 for non-relativistic electrons and protons. Then from equation (16), we obtain the equation for $T_{\rm i}$,

$$\frac{3}{2}\frac{{\rm d}T_{\rm i}}{{\rm d}r} = \frac{T_{\rm i}}{n}\frac{{\rm d}n}{{\rm d}r} + \frac{1}{kn}\frac{{\rm d}Q_{\rm i}}{{\rm d}t'}\frac{1}{c\,\Gamma_{\rm p}\,\beta_{\rm p}}, \qquad {\rm i} = {\rm e},\, {\rm p}, \tag{18}$$

where d $t' =$ d $t/\Gamma_{\rm p}$ is time measured in the fluid frame. Electrons exchange energy with photons via Compton scattering and with protons via Coulomb collisions,

$$\frac{{\rm d}Q_{\rm e}}{{\rm d}t'} = \frac{3}{2}nk\left(\frac{T_{\rm c} - T_{\rm e}}{\tau_{\rm c}} + \frac{T_{\rm p} - T_{\rm e}}{\tau_{\rm ep}}\right), \tag{19}$$

where

$$\tau_{\rm ep} = \sqrt{\frac{\pi}{2}}\,\frac{m_{\rm p}}{m_{\rm e}}\,\frac{1}{\sigma_{\rm T}\,c\,\ln\Lambda}\,\frac{1}{n_{\rm e}}\left(\frac{k\,T_{\rm e}}{m_{\rm e}c^2}+\frac{k\,T_{\rm p}}{m_{\rm p}c^2}\right)^{3/2} \tag{20}$$

is the Coulomb time-scale (with Coulomb logarithm $\ln\Lambda \simeq 15$; see Stepney 1983),

$$\tau_{\rm c} = \frac{3\,m_{\rm e}\,c}{8\,U_{\rm rad}\sigma_{\rm T}} \tag{21}$$

is the Compton time-scale,

$$U_{\rm rad} = a\,T_{\rm r}^4$$

is the radiation energy density and $T_{\rm C}$ is the Compton temperature of radiation. For blackbody radiation $T_{\rm C} = T_{\rm r}$.

The thermal balance for protons reads

$$\frac{{\rm d}Q_{\rm p}}{{\rm d}t'} = -\frac{3}{2}nk\frac{(T_{\rm p}-T_{\rm e})}{\tau_{\rm ep}}. \tag{22}$$

We have neglected here the energy exchange between protons and radiation; it is $\sim(m_{\rm e}/m_{\rm p})^3$ times the electron-radiation energy exchange.

2.2 Transparent stage

Electron scattering dominates opacity of the outflow, and its optical depth is

$$\tau_{\rm T} = \frac{n_{\rm e}\,\sigma_{\rm T}\,r}{\Gamma_{\rm p}} = \frac{L\,\sigma_{\rm T}}{4\pi r m_{\rm p}c^3\,\Gamma_{\rm p}^2\,\eta}, \tag{23}$$

where $n_{\rm e} = n$ is the electron number density. At radii $r > R_\tau$ where $\tau_{\rm T} < 1$, the outflow is transparent and equation (8) is no longer valid. The photon luminosity at this point is (see equation 6)

$$L_\gamma = \frac{16\pi}{3}R_\tau^2 c\beta_{\rm p}\Gamma_{\rm p}^2 a T_{\rm r}^4, \tag{24}$$

where all quantities are taken at $r = R_\tau$. Approximately this luminosity escapes to a distant observer as a blackbody radiation with observed temperature $\Gamma_{\rm p}T_{\rm r}(R_\tau)$.

2.2.1 Outflow acceleration

After the transparency radius, the outflow may still be accelerated by radiation.

A freely propagating photon at an angle θ with respect to radius satisfies the relation $r\sin\theta = {\rm const}$ and becomes more beamed at larger r. A typical photon is emitted at angle $\pi/2$ in the plasma frame and has initial beaming angle $\theta_{\rm rad} \approx 1/\Gamma_{\rm p}$ at $r = R_\tau$. At larger radii the beaming angle decreases as

$$\theta_{\rm rad} \approx \frac{R_\tau}{r}\frac{1}{\Gamma_{\rm p}(R_\tau)}. \tag{25}$$

One can define a frame where the freely streaming radiation remains approximately isotropic. The velocity of this frame is $\beta_{\rm rad} = \cos\theta_{\rm rad}$ and its Lorentz factor is

$$\Gamma_{\rm rad} = \frac{1}{\sin\theta_{\rm rad}} \approx \frac{r}{R_\tau}\Gamma_{\rm p}(R_\tau). \tag{26}$$

The streaming radiation will tend to accelerate the plasma outflow since $\Gamma_{\rm rad} > \Gamma_{\rm p}$. The radiation flux $F_\gamma = L_\gamma/4\pi r^2$ exerts a force on an electron moving with velocity $\beta_{\rm p}$ (see Beloborodov 2002, equation A6),

$$\frac{{\rm d}p}{{\rm d}t} = \frac{\sigma_{\rm T}F_\gamma}{c}\left(\frac{1-\beta_{\rm p}}{1+\beta_{\rm p}}\right)\left(1-\frac{\Gamma_{\rm p}^4}{\Gamma_{\rm rad}^4}\right), \tag{27}$$

and the plasma Lorentz factor grows,

$$\frac{{\rm d}\Gamma_{\rm p}}{{\rm d}r} = \frac{\sigma_{\rm T}L_\gamma}{16\pi r^2 m_{\rm p}c^3\Gamma_{\rm p}^2}\left(1-\frac{\Gamma_{\rm p}^4}{\Gamma_{\rm rad}^4}\right). \tag{28}$$

An easy estimate of the acceleration effect may be obtained neglecting the factor $\Gamma_{\rm p}^4/\Gamma_{\rm rad}^4$ in parenthesis. Then equation (28) gives

$$\Gamma_{\rm p}^3(r) = \Gamma_{\rm p}^3(R_\tau) + \frac{3\sigma_{\rm T}L_\gamma}{16\pi m_{\rm p}c^3}\left(\frac{1}{R_\tau}-\frac{1}{r}\right). \tag{29}$$

The acceleration at the transparent stage is significant if at $r \gg R_\tau$ the second term on right-hand side exceeds the first term. This condition is equivalent to $aT_{\rm r}^4 > nm_{\rm p}\,c^2$ at $r = R_\tau$, which requires most of the outflow energy be in radiation at the moment of transparency. The same condition may be expressed in terms of η (e.g. Mészáros & Rees 2000b),

$$\eta > \eta_{\rm rad} \approx \left(\frac{L\sigma_{\rm T}}{4\pi\,R_0 m_{\rm p}c^3}\right)^{1/4} \approx 10^3\,L_{52}^{1/4}\,R_{0,7}^{-1/4}. \tag{30}$$

2.2.2 Thermal balance

The thermal balance of the outflow at the transparent stage is still given by equations (18), (19) and (22). The Coulomb time-scale is given by the same equation (20) and the Compton time-scale is given by equation (21) with

$$U_{\rm rad}(r) \approx \frac{L_\gamma}{4\pi r^2 c\Gamma_{\rm p}^2} \tag{31}$$

being the radiation density measured in the plasma frame.

We note that the outflow is subject to significant Compton cooling even at $r > R_\tau$ because the scattering rate *per electron* is still very high at R_τ (it is $n_\gamma/n \sim 10^5$ higher than the scattering rate per photon). The Compton temperature $T_{\rm C}$ appearing in equation (19) represents the effective temperature of radiation observed from the plasma frame and is proportional to the average photon energy in this frame. $T_{\rm C}$ may be evaluated as follows.

The typical photon at $r > R_\tau$ has angle $\theta(r) = \theta_{\rm rad}(r)$ and constant energy $\epsilon(r) = \epsilon'(R_\tau)\Gamma_{\rm p}(R_\tau)$ in the lab frame. Its energy in the plasma frame is

$$\epsilon'(r) = \epsilon\Gamma_{\rm p}(1-\beta_{\rm p}\cos\theta_{\rm rad}) = \epsilon\Gamma_{\rm p}(1-\beta_{\rm p}\beta_{\rm rad})$$
$$\approx \epsilon'(R_\tau)\Gamma_{\rm p}(R_\tau)\frac{1}{2}\left(\frac{1}{\Gamma_{\rm p}}+\frac{\Gamma_{\rm p}}{\Gamma_{\rm rad}^2}\right).$$

The Compton temperature changes with radius as

$$\frac{T_{\rm C}(r)}{T_{\rm C}(R_\tau)} = \frac{\epsilon'(r)}{\epsilon'(R_\tau)} \approx \frac{1}{2}\frac{\Gamma_{\rm p}(R_\tau)}{\Gamma_{\rm p}(r)}\left[1+\frac{\Gamma_{\rm p}^2(r)}{\Gamma_{\rm rad}^2(r)}\right], \tag{32}$$

where $T_{\rm C}(R_\tau) = T_{\rm r}(R_\tau)$. Equation (32) completes the description of Compton energy exchange at the transparent stage.

2.3 Numerical models

Numerical models of outflows with $\eta = 200$ and 800 are shown in Figs 1 and 2. Both models have $\eta < \eta_{\rm rad}$ and the outflow Lorentz factor saturates before transparency.

Upper panels in Figs 1 and 2 show the evolution of the Lorentz factor. As long as enthalpy exceeds rest-mass energy ($x > 1$), the outflow accelerates with $\Gamma_{\rm p} \propto r$. When most of the internal energy is converted to kinetic energy ($x < 1$) $\Gamma_{\rm p}$ tends to a constant asymptotic

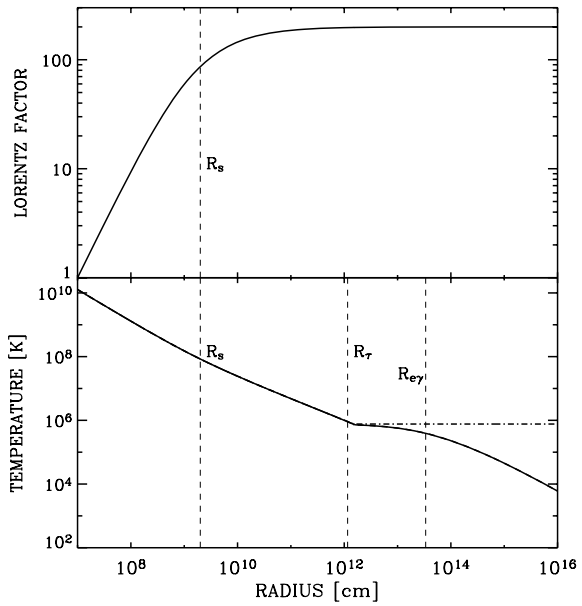

Figure 1. Lorentz factor (upper panel) and temperature (lower panel) as functions of radius for a neutron-free outflow with $L = 10^{52}\,\mathrm{erg\,s^{-1}}$, $\eta = 200$ and $R_0 = 10^7$ cm. Electrons never decouple thermally from protons and their common temperature is shown by the solid curve. Dash–dotted curve shows the radiation temperature.

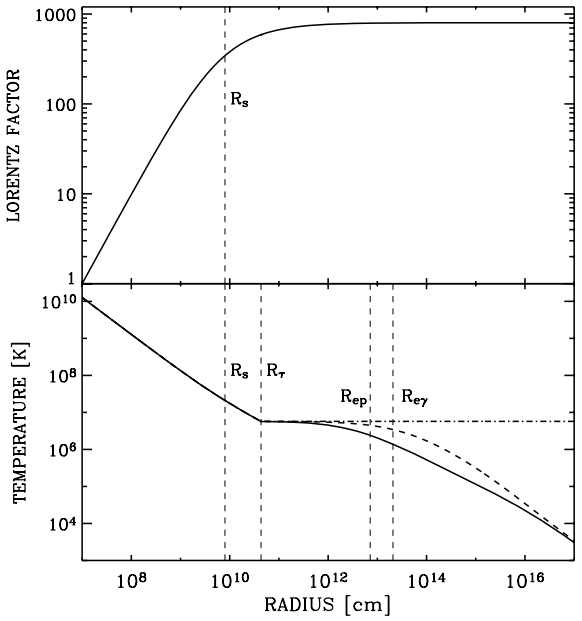

Figure 2. Same as Fig. 1 but for $\eta = 800$. T_p and T_e are shown by solid and dashed curves, respectively. The thermal decoupling $T_\mathrm{e} > T_\mathrm{p}$ takes place at radii $r \sim 10^{12}$–10^{16} cm.

value $\Gamma_\mathrm{pf} = \eta$. The characteristic saturation radius R_s is where $x = 1$; $\Gamma_\mathrm{p} = \eta/2$ at this radius and

$$R_\mathrm{s} = 2^{-1/4}\eta R_0. \tag{33}$$

Solutions for temperatures T_r, T_e and T_p are shown in the lower panels of Figs 1 and 2. At very small radii where $kT \gtrsim m_\mathrm{e}c^2 = 511$ keV, the number density of $e^\pm$ pairs is comparable to that of photons, the energy density is $(11/4)aT_\mathrm{r}^4$ and the temperature is reduced by the factor of $(4/11)^{1/4} \approx 0.78$; this correction is neglected in the figures. As long as the outflow is optically thick, all three components maintain a common temperature T via Coulomb collisions and Compton scattering, and T decreases adiabatically with index $\hat{\gamma} = 4/3$. The outflow becomes transparent at radius

$$R_\tau = \frac{L\sigma_\mathrm{T}}{4\pi m_\mathrm{p}c^3\Gamma_\mathrm{pf}^3}, \qquad \eta < \eta_\mathrm{rad}. \tag{34}$$

At the transparent stage the plasma is still tracking the temperature of (freely streaming) photons: $T_\mathrm{e} \approx T_\mathrm{p} \approx T_\mathrm{r} \approx$ const until the electrons decouple either from radiation (e–γ decoupling) or from the protons (e–p decoupling).

The e–γ decoupling occurs at a radius $R_{e\gamma}$ where the Compton time-scale (equation 21) exceeds the expansion time-scale $\tau_\mathrm{exp} = R/\Gamma_\mathrm{p}\,c$,

$$R_{e\gamma} = \frac{2}{3\pi}\frac{L_\gamma\sigma_\mathrm{T}}{m_\mathrm{e}c^3\Gamma_\mathrm{pf}^3} \approx \frac{2\sigma_\mathrm{T}L}{3\pi m_\mathrm{e}c^3\,\eta^{7/3}}\left(\frac{R_0}{R_\tau}\right)^{2/3}. \tag{35}$$

The e–p decoupling may happen or not depending mostly on the value of η. The two possible cases are illustrated in Figs 1 and 2.

(i) Electrons and protons are still coupled at $R_{e\gamma}(\tau_\mathrm{ep} < \tau_\mathrm{exp})$ and begin a common adiabatic cooling, $T_\mathrm{p} = T_\mathrm{e} \propto n_\mathrm{e}^{2/3}$. They will not decouple later because $\tau_\mathrm{ep} =$ const while τ_exp keeps increasing. This regime takes place at $\eta \lesssim 650$ and is illustrated in Fig. 1.

(ii) Electrons decouple from protons before $R_{e\gamma}$. The radius of e–p decoupling is found from condition $\tau_\mathrm{ep} = \tau_\mathrm{exp}$. Using $T_\mathrm{e} \approx T_\mathrm{r}(R_\tau) = T_\mathrm{r}(R_\mathrm{s})(R_\tau/R_\mathrm{s})^{-3/2}$ in equation (20) for τ_ep (and neglecting the small term $kT_\mathrm{p}/m_\mathrm{p}c^2$), we get

$$R_\mathrm{ep} \simeq \left(68\pi m_\mathrm{p}c^4\right)^{-1}\frac{L}{\eta^3\,T_\mathrm{s}^{3/2}}\left(\frac{R_\tau}{R_\mathrm{s}}\right), \tag{36}$$

where $T_\mathrm{s} = 2T_0/\eta$ is the temperature at the saturation radius. At $R_\mathrm{ep} < r < R_{e\gamma}$, $T_\mathrm{e} \approx T_\mathrm{r} > T_\mathrm{p}$. At $r > R_{e\gamma}$, the electrons cool down adiabatically and $\tau_\mathrm{ep} \approx$ const while τ_exp keeps increasing. Therefore, electrons and protons eventually regain the thermal coupling. This regime takes place at high $\eta \gtrsim 650$ and is illustrated in Fig. 2.

Fig. 3 shows a model with $\eta = 8 \times 10^3 > \eta_\mathrm{rad}$. In this case, the outflow acceleration continues after the transparency radius

$$R_\tau \simeq R_0\,\eta_\mathrm{rad}\left(\frac{\eta_\mathrm{rad}}{\eta}\right)^{1/3}, \qquad \eta > \eta_\mathrm{rad}, \tag{37}$$

and Γ_p saturates at

$$\Gamma_\mathrm{pf} \approx \eta_\mathrm{rad}\left(\frac{\eta}{\eta_\mathrm{rad}}\right)^{1/9} < \eta, \tag{38}$$

after a few R_τ. Since density is lower than in the previous examples, the e–p decoupling happens much earlier than the e–γ decoupling ($R_\mathrm{ep} \ll R_\gamma$).

In summary, the thermal evolution of a neutron-free outflow is dominated by adiabatic cooling. The opaque outflow has a common temperature $T_\mathrm{p} = T_\mathrm{e} = T_\mathrm{r}$ which decreases as r^{-1} during the acceleration stage and as $r^{-2/3}$ during the coasting stage. Then, after an intermediate stage where the details of coupling between e and p, and radiation are important, the outflow is again described by a simple adiabatic law $T_\mathrm{p} \approx T_\mathrm{e} \propto r^{-4/3}$. The presence of neutrons will change this picture.

3 NEUTRON-LOADED OUTFLOW

We now consider an outflow with a neutron component and denote its initial neutron richness (neutron-to-proton ratio) by ξ_0. All other

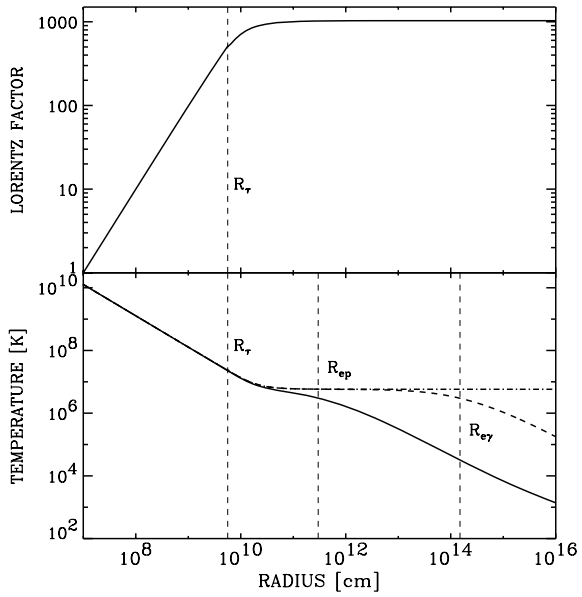

Figure 3. Same as Fig. 2 but for $\eta = 8 \times 10^3$. The outflow becomes transparent before the acceleration stage ends.

assumptions are the same as in Section 2. In particular, we consider spherical expansion driven by radiation pressure. Neutrons and protons are injected at $r = R_0$ with an initial density ratio $\xi = \xi_0$, and then ξ evolves with radius because neutrons continuously β decay into protons,

$$n \rightarrow p + e + \bar{\nu}.$$

The mean lifetime of neutrons in their rest frame is $\tau_\beta \approx 900\,\mathrm{s}$, and the corresponding mean radius of β decay is

$$R_\beta = \int_0^{\tau_\beta} c\beta_\mathrm{n}\Gamma_\mathrm{n}\,\mathrm{d}\tau \simeq 8 \times 10^{15}\left(\frac{\Gamma_\mathrm{nf}}{300}\right)\ \mathrm{cm}, \tag{39}$$

where Γ_n is the neutron Lorentz factor and $\beta_\mathrm{n} \approx 1$; Γ_nf is the final value of Γ_n achieved at $r \sim (10^2\text{–}10^3)R_0 \ll R_\beta$. The neutron population is gradually depleted as $\exp(-r/R_\beta)$ and the *n*/*p* ratio (measured in the fixed lab frame) evolves with radius as

$$\xi \equiv \frac{\Gamma_\mathrm{n} n_\mathrm{n}}{\Gamma_\mathrm{p} n_\mathrm{p}} = \frac{\xi_0 \mathrm{e}^{-r/R_\beta}}{1 + \xi_0\left(1 - \mathrm{e}^{-r/R_\beta}\right)}, \tag{40}$$

where n_n and n_p are proper densities of the neutron and proton components.

3.1 Outflow acceleration and *n–p* coupling

The total luminosity of the outflow (cf. equation 6) now includes the contribution from neutrons,

$$L = 4\pi r^2 c\left[\beta_\mathrm{p}\Gamma_\mathrm{p}^2\left(\frac{4}{3}a\,T_\mathrm{r}^4 + \rho_\mathrm{p}\,c^2\right) + \beta_\mathrm{n}\Gamma_\mathrm{n}^2\rho_\mathrm{n}c^2\right] = \mathrm{const}, \tag{41}$$

where $\rho_\mathrm{p} = n_\mathrm{p}\,m_\mathrm{p}$ and $\rho_\mathrm{n} = n_\mathrm{n}\,m_\mathrm{n}$; the thermal energy of the plasma and neutrons has been neglected compared to their rest-mass energy. We allow here the neutron component to have a different Lorentz factor Γ_n, which will be close to Γ_p as long as the *n–p* coupling is efficient.

The baryon outflow rate is given by

$$\dot{M} = 4\,\pi r^2\,c(\beta_\mathrm{p}\Gamma_\mathrm{p}\rho_\mathrm{p} + \beta_\mathrm{n}\Gamma_\mathrm{n}\rho_\mathrm{n}) = \mathrm{const}. \tag{42}$$

The outflow expansion is accompanied by adiabatic cooling which determines $T_\mathrm{r}(r)$. Expansion of volume can be described by the decrease of number density of *original* protons injected at the base of the outflow. We denote this density by n and distinguish it from the total proton density n_p that includes the decayed neutrons. They are related by

$$n_\mathrm{p} = n\,\frac{1+\xi_0}{1+\xi}. \tag{43}$$

The radiation temperature at the optically thick stage obeys equation (8). We neglect destruction of neutrons at this stage (see Section 3.6) and assume in this section $\xi = \xi_0$ and $n = n_\mathrm{p}$. The difference between n_p and n will become significant at larger radii comparable to R_β.

Acceleration of the optically thick outflow is described by equations (41), (42) and (8), from which we derive

$$\frac{\mathrm{d}\Gamma_\mathrm{p}}{\mathrm{d}r} = \frac{\Gamma_\mathrm{p}}{r}\frac{2x}{2x+3} - \frac{\mathrm{d}\Gamma_\mathrm{n}}{\mathrm{d}r}\frac{3\xi_0}{2x+3}, \tag{44}$$

where

$$x = \frac{4}{3}\frac{aT_\mathrm{r}^4}{n_\mathrm{p}m_\mathrm{p}c^2} = x_0\left(\frac{n}{n_0}\right)^{1/3}, \qquad x_0 = \frac{\eta(1+\xi_0)}{\Gamma_0} - 1, \tag{45}$$

$$x(r) = x_0\left(\frac{r}{R_0}\right)^{-2/3}\left(\Gamma_\mathrm{p}\beta_\mathrm{p}\right)^{-1/3}. \tag{46}$$

The first term on the right-hand side of equation (44) describes the acceleration by radiation pressure; the second term describes the deceleration caused by transfer of momentum to neutrons.

As long as the collisional *n–p* coupling is strong, $\Gamma_\mathrm{n} \approx \Gamma_\mathrm{p}$, equation (44) yields

$$\frac{\mathrm{d}\Gamma_\mathrm{p}}{\mathrm{d}r} = \frac{\Gamma_\mathrm{p}}{r}\frac{2x}{2x+3(1+\xi_0)}. \tag{47}$$

Acceleration of coupled *n* and *p* begins to saturate when $x \approx 1 + \xi_0$ at a radius

$$R_\mathrm{sb} \approx \eta R_0, \qquad \Gamma_\mathrm{p}(R_\mathrm{sb}) \approx \frac{\eta}{2}. \tag{48}$$

At that point $\rho_\mathrm{b}c^2 \approx aT_\mathrm{r}^4$, where $\rho_\mathrm{b} \approx \rho_\mathrm{p} + \rho_\mathrm{n}$. In the case of $\xi_0 \gg 1$, acceleration saturates when x is still large because the protons are coupled to a large number of neutrons and have a lot of effective inertia. Decoupling from neutrons at $r \lesssim R_\mathrm{sb}$ would allow the protons to accelerate further and reach Lorentz factors $\Gamma_\mathrm{p} \sim \eta(1+\xi_0)$ if the outflow remains optically thick (Fuller, Pruet & Abazajian 2000).

Description of *n–p* decoupling will require one more equation that specifies momentum exchange between neutron and proton components. Neutrons accelerate because they collide with the accelerating protons. In its rest frame, a neutron experiences $\Gamma_\mathrm{rel} n_\mathrm{p}\sigma_\mathrm{np}c$ collisions per second, [2] where $\sigma_\mathrm{np} \approx 3 \times 10^{-26}\,\mathrm{cm}^2$ and

$$\Gamma_\mathrm{rel} = \Gamma_\mathrm{p}\Gamma_\mathrm{n}\left(1 - \beta_\mathrm{p}\beta_\mathrm{n}\right) \approx \frac{1}{2}\left(\frac{\Gamma_\mathrm{p}}{\Gamma_\mathrm{n}} + \frac{\Gamma_\mathrm{n}}{\Gamma_\mathrm{p}}\right) \tag{49}$$

is the Lorentz factor of the neutron component relative to the plasma component. Assuming isotropic scattering in the center-of-momentum frame, the mean momentum gained by the neutron per collision equals $\tilde{p}_\mathrm{p} = \mu v_\mathrm{rel}\Gamma_\mathrm{rel}$, where $\mu = m_\mathrm{p}\,m_\mathrm{n}/(m_\mathrm{n} + m_\mathrm{p}) \approx$

[2] To the first approximation the rate of *n–p* collisions $\langle\sigma\,v\rangle$ does not depend on the relative velocity v of colliding particles and one may take $\langle\sigma\rangle = \langle\sigma_\mathrm{np}\,c\rangle$.

$m_p/2$ is the reduced mass. The momentum gained by a neutron during time $d\tilde{t}$ is

$$d\tilde{p}_n = \frac{1}{2}\, n_p \Gamma_{rel}^2 \sigma_{np} \beta_{rel} m_p c^2\, d\tilde{t}. \tag{50}$$

The corresponding change of the neutron Lorentz factor in the lab frame is found from the Lorentz transformation of four-momentum $d\tilde{p}_n^\alpha = (0, d\tilde{p}_n)$,

$$d\Gamma_n = \Gamma_n \beta_n \frac{d\tilde{p}_n}{m_n c}, \tag{51}$$

and one gets

$$\frac{d\Gamma_n}{dr} = \frac{1}{2}\, n_p \Gamma_{rel}^2 \beta_{rel} \sigma_{np}. \tag{52}$$

Equation (52) closes the set of dynamic equations describing the outflow acceleration at the optically thick stage.

The collisional coupling between the proton and neutron components is friction, which inevitably dissipates energy and heats both components. This heating will be included in the plasma thermal balance below (Section 3.5).

3.2 *n–p* decoupling and transparency

As long as the *n–p* coupling is efficient, $\Gamma_p \approx \Gamma_n$, the relative velocity $\beta_{rel} \ll 1$ may be evaluated using equations (47) and (52),

$$\beta_{rel} \approx \frac{2\Gamma_p}{n_p \sigma_{np} r} \frac{2x}{2x + 3(1+\xi_0)} = \frac{2\Gamma_p}{n_p \sigma_{np} r} \frac{1}{1 + (9/8)\rho_b c^2 / a T_r^4}. \tag{53}$$

The decoupling of Γ_n from Γ_p may happen at $r \lesssim R_{sb}$ where $aT_r^4 > \rho_b c^2$, and according to equation (53)

$$\beta_{rel} \approx \frac{2\Gamma_p}{n_p \sigma_{np} r}, \qquad r < R_{sb}. \tag{54}$$

The decoupling condition is expressed by setting $\beta_{rel} = 1$ in equation (54). The β_{rel} approaches unity at $r \lesssim R_{sb}$ if the outflow has a sufficiently high η,

$$\eta > \eta_* \approx \left[\frac{L\sigma_{np}}{4\pi R_0 m_p c^3 (1+\xi_0)}\right]^{1/4} = \frac{4.8\times 10^2}{(1+\xi_0)^{1/4}} \left(\frac{L_{52}}{R_{0,7}}\right)^{1/4}. \tag{55}$$

Then the decoupling radius is given by

$$R_{np} \approx \left[\frac{L\sigma_{np}}{8\pi R_0 \eta m_p c^3 (1+\xi_0)}\right]^{1/3} R_0, \tag{56}$$

and the neutron Lorentz factor at decoupling is

$$\Gamma_{nf} \approx \frac{R_{np}}{R_0} \approx \frac{\eta_*^{4/3}}{\eta^{1/3}}, \qquad \eta > \eta_*. \tag{57}$$

No significant decoupling $\Gamma_p > \Gamma_n$ happens for $\eta < \eta_*$. This is so despite the fact that $\eta < \eta_*$ does not exclude $\rho_p c^2 < aT_r^4 < \rho_b c^2$ at $r > R_{sb}$, so there may be enough energy in radiation to accelerate protons to $\Gamma_p > \Gamma_{nf}$. A detailed analysis and numerical models show that if β_{rel} is small at $r \lesssim R_{sb}$, it remains small at $r > R_{sb}$. Therefore, to a good approximation, $\eta > \eta_*$ may be taken as a true condition for decoupling of Γ_p from Γ_n (see also Bahcall & Mészáros 2000). Hereafter we focus on $\eta > \eta_*$.

The decoupled neutrons do not affect the remaining *e–p–γ* outflow until a much larger radius where β decay becomes important (see below). Therefore, saturation of proton acceleration and transition to transparency may be described as if there were no neutrons. This 'neutron-free' outflow has luminosity

$$\hat{L} = L - \Gamma_{nf} \dot{M} c^2 \frac{\xi_0}{1+\xi_0}, \tag{58}$$

and mass outflow rate

$$\hat{M} = \frac{\dot{M}}{1+\xi_0}. \tag{59}$$

Equations of Section 2 then apply if one replaces $L \to \hat{L}$, $\dot{M} \to \hat{M}$ and $\eta \to \hat{\eta} = \hat{L}/\hat{M}c^2$.

The outflow is still opaque to radiation at the *n–p* decoupling radius. This follows from the small ratio of cross-sections $\sigma_{np}/\sigma_T \sim 1/20$. If $e^\pm$ cascade initiated by π^0 is neglected (see DKK99a and Section 3.7), transparency comes soon after R_{np}. In this case, one can show that an outflow with $\Gamma_p > \Gamma_n (\eta > \eta_*)$ becomes transparent before saturation of Γ_p. This may be seen from the following relation:

$$\frac{\hat{\eta}}{\hat{\eta}_{rad}} = \left[1 + \xi_0 \left(1 - \frac{\Gamma_{nf}}{\eta}\right)\right]^{3/4} \left(\frac{\sigma_T}{\sigma_{np}}\right)^{1/4} \frac{\eta}{\eta_*}, \tag{60}$$

where (cf. equation 30)

$$\hat{\eta}_{rad} = \left(\frac{\hat{L}\sigma_T}{4\pi R_0 m_p c^3}\right)^{1/4}. \tag{61}$$

$\eta > \eta_*$ implies $\hat{\eta} > \hat{\eta}_{rad}$ and hence Γ_p does not reach the maximum possible value $\Gamma_{p,max} = \hat{\eta}$. The outflow becomes transparent and Γ_p saturates at (cf. equation 38)

$$\Gamma_{pf} \approx \hat{\eta}_{rad} \left(\frac{\hat{\eta}}{\hat{\eta}_{rad}}\right)^{1/9}. \tag{62}$$

It is not much larger than Γ_{nf}. The $e^\pm$ cascade initiated by π^0 decay may prolong the opaque stage and increase Γ_{pf}.

3.3 Deceleration by β decay

Next, we consider larger radii $r > R_\tau$ when the outflow is composed of decoupled radiation with luminosity L_γ, decoupled neutrons and plasma. The neutrons are no longer a fluid; they retain a mildly relativistic velocity dispersion acquired at their last collisions at $r \sim R_{np}$, which implies that Γ_n varies by a factor of <2. We will neglect this dispersion and assume that all neutrons have equal Lorentz factors Γ_n after decoupling.

The neutrons continuously β decay in the outflow and create a source of protons and electrons moving with respect to the plasma frame with a Lorentz factor Γ_{rel}. This beam shares momentum with the plasma, heats it and reduces the plasma Lorentz factor Γ_p.

The outflow luminosity at the transparent stage may be approximated as

$$L = 4\pi r^2 c \left[\beta_p \Gamma_p^2 (\rho_p c^2 + h_p) + \beta_n \Gamma_n^2 \rho_n c^2\right] + L_\gamma = \text{const}. \tag{63}$$

We include here the enthalpy of proton component $h_p = U_p + P_p$ for completeness. As we shall see the plasma is heated to a high temperature at large radii $r \sim R_\beta$, however, h_p remains smaller than $\rho_p c^2$. The enthalpy is related to proton temperature by

$$h_p = \frac{\hat{\gamma}}{\hat{\gamma} - 1} n_p k T_p, \tag{64}$$

where $\hat{\gamma}$ is the adiabatic index of the proton component, which is between 4/3 and 5/3. From equations (42), (63) and using the first

law of thermodynamics (equations 16 and 17), we derive

$$\frac{\mathrm{d}\Gamma_\mathrm{p}}{\mathrm{d}r} = \frac{1}{1+x_\mathrm{p}(2-\hat{\gamma})}\left[\frac{\xi(\Gamma_\mathrm{n}-\Gamma_\mathrm{p})}{R_\beta} + \frac{2(\hat{\gamma}-1)}{r}\Gamma_\mathrm{p}x_\mathrm{p} - \frac{\Gamma_\mathrm{p}\hat{\gamma}}{\rho_\mathrm{p}c^2}\frac{\mathrm{d}q_\mathrm{p}}{\mathrm{d}r} - \frac{\Gamma_\mathrm{p}x_\mathrm{p}}{\hat{\gamma}}\frac{d\hat{\gamma}}{\mathrm{d}r}\right] + \frac{\sigma_\mathrm{T}L_\gamma}{16\pi r^2 m_\mathrm{p}c^3\Gamma_\mathrm{p}^2}\left(1-\frac{\Gamma_\mathrm{p}^4}{\Gamma_\mathrm{rad}^4}\right), \quad (65)$$

where $x_\mathrm{p} = h_\mathrm{p}/\rho_\mathrm{p}c^2$. The last term describes the radiative acceleration (see Section 2.2.1).

3.4 Summary of the dynamical model

Our dynamical model of the neutron-loaded outflow may be summarized as follows. It is described by different equations before and after transparency, and the equations match at the transparency radius. Before transparency, $r < R_\tau$, we neglect the decay of neutrons. The evolution of Γ_p and Γ_n is found from equations (44) and (52).

After transparency, $r > R_\tau$, we neglect the *n–p* collisions and assume $\Gamma_\mathrm{n} = \mathrm{const}$. We take into account the β decay which becomes increasingly important at larger radii. The evolution of Γ_p is described by equation (65). It includes the heating term $\mathrm{d}q_\mathrm{p}/\mathrm{d}r$ which may be non-negligible at $r \sim R_\beta$. This term couples the dynamics with the proton thermal balance which is discussed in Section 3.5.

The two descriptions match at the beginning of the coasting phase $(\mathrm{d}\Gamma_\mathrm{p}/\mathrm{d}r) = 0$ where neither *n–p* collisions nor β decay affects the outflow.

3.5 Thermal balance

Thermal evolution of electrons and protons obeys the first law of thermodynamics (equation 16). Using equations (17) and (43), we derive

$$(1+\xi)\frac{\mathrm{d}}{\mathrm{d}r}\left[\frac{T_\mathrm{i}}{(\hat{\gamma}-1)(1+\xi)}\right] = \frac{T_\mathrm{i}}{n}\frac{\mathrm{d}n}{\mathrm{d}r} + \frac{1}{kn_\mathrm{p}}\frac{\mathrm{d}Q_\mathrm{i}}{\mathrm{d}t'}\frac{1}{c\,\Gamma_\mathrm{p}\beta_\mathrm{p}}. \quad (66)$$

Here $\mathrm{d}Q_\mathrm{i}/\mathrm{d}t'$ (i = e, p) are the heating rates of electrons and protons.

The thermal balance of protons is significantly changed compared to the neutron-free case because of two effects: (i) frictional heating due to *n–p* collisions and (ii) heating due to β decay.

The rate of *n–p* collisions per unit volume in the plasma frame is

$$\dot{n}_\mathrm{ep} = n'_\mathrm{n}n_\mathrm{p}\sigma_\mathrm{np}c,$$

where $n'_\mathrm{n} = \Gamma_\mathrm{rel}n_\mathrm{n}$ is neutron density measured in the plasma frame. The mean energy dissipated per collision is $(1/2)(\Gamma_\mathrm{rel}-1)m_\mathrm{p}c^2$ assuming that the relative bulk velocity is isotropized in collisions. This gives the frictional heating rate,

$$\frac{\mathrm{d}Q_\mathrm{np}}{\mathrm{d}t'} = \frac{1}{2}\Gamma_\mathrm{rel}(\Gamma_\mathrm{rel}-1)m_\mathrm{p}c^3\sigma_\mathrm{np}n_\mathrm{n}n_\mathrm{p}. \quad (67)$$

Heating also results from the gradual β decay of the neutron component. The decay rate per unit volume is Lorentz invariant and in the plasma frame (where the decay time is $\Gamma_\mathrm{rel}\,\tau_\beta$) may be written as

$$\dot{n}_\beta = \frac{n'_\mathrm{n}}{\Gamma_\mathrm{rel}\tau_\beta} = \frac{n_\mathrm{n}}{\tau_\beta}. \quad (68)$$

The decay products form an $e-p$ beam with velocity v_rel in the plasma frame, which immediately dissipates its relative kinetic energy into heat. We will assume that this heat goes entirely to the proton component. The dissipated energy per decayed neutron is $(\Gamma_\mathrm{rel}-1)m_\mathrm{p}c^2$, which gives the heating rate,

$$\frac{\mathrm{d}Q_\beta}{\mathrm{d}t'} = (\Gamma_\mathrm{rel}-1)\,m_\mathrm{p}c^2\frac{n_\mathrm{n}}{\tau_\beta}. \quad (69)$$

Protons also exchange energy with electrons via Coulomb collisions with rate $\mathrm{d}Q_\mathrm{ep}/\mathrm{d}t'$ (equation 22). The net thermal balance of the proton component is then given by

$$\frac{\mathrm{d}q_\mathrm{p}}{\mathrm{d}t'} = -\frac{\mathrm{d}Q_\mathrm{ep}}{\mathrm{d}t'} + \Gamma_\mathrm{rel}n_\mathrm{n}\,(\Gamma_\mathrm{rel}-1)\,m_\mathrm{p}c^2\left(\frac{1}{2}\,n_\mathrm{p}\sigma_\mathrm{np}c + \frac{1}{\Gamma_\mathrm{rel}\tau_\beta}\right). \quad (70)$$

The β decay weakly affects the plasma thermal balance as long as $(\Gamma_\mathrm{rel}\,\tau_\beta)^{-1} \ll n_\mathrm{p}\,\sigma_\mathrm{np}c$. The decay becomes important at large radii, after the outflow becomes transparent.

The thermal-balance equation for electrons is similar to the neutron-free case (Section 2),

$$\frac{\mathrm{d}Q_\mathrm{e}}{\mathrm{d}t'} = \frac{3}{2}\,n_\mathrm{p}k\frac{(T_\mathrm{c}-T_\mathrm{e})}{\tau_\mathrm{c}} + \frac{\mathrm{d}Q_\mathrm{ep}}{\mathrm{d}t'}. \quad (71)$$

3.6 Destruction of neutrons by inelastic collisions

We assume in this paper that neutron richness ξ changes only as a result of β decay and neglect other channels of neutron conversion to protons. In fact, near the decoupling radius R_np the collisions between neutrons and protons become sufficiently energic to produce pions (DKK99a). Thus, some collisions are inelastic, which may destroy the neutron component.

Inelastic *n–p* collisions may convert neutron to proton $n+p \to p+p+\pi^-$ as well as proton to neutron $n+p \to n+n+\pi^+$. These reactions have equal cross-section which has been measured down to the 140 MeV threshold (e.g. Daum et al. 2002). The reactions have equal rates and do not change neutron richness ξ.

Inelastic *n–n* collisions may destroy the neutron component via reactions $n+n \to d+\pi^-$ and $n+n \to n+p+\pi^-$. These reactions have same cross-sections as reactions $p+p \to d+\pi^+$ and $p+p \to n+p+\pi^+$, respectively, which have been studied in experiments (Shimizu et al. 1982). The cross-section of $d\pi^-$ channel does not exceed 0.1 of the elastic cross-section and is less important. The main reaction of neutron destruction is $n+n \to n+p+\pi^-$. Its cross-section becomes comparable to the elastic cross-section when neutrons collide with relative energy $E_\mathrm{nn} > 700\,\mathrm{MeV}$ and quickly decreases at smaller E_nn.

The rate of elastic *n–n* collisions is ξ times higher than the rate of *n–p* collisions, which equals the expansion rate at decoupling. Therefore, the time-scale of *n–n* collisions at $r \sim R_\mathrm{np}$ is ξ^{-1} times shorter than the expansion time τ_exp, and at large ξ neutrons may be treated as Maxwellian gas. This gas is heated by *n–p* collisions which dissipate energy $(\Gamma_\mathrm{rel}-1)m_\mathrm{p}c^2/2 \approx m_\mathrm{p}\,v_\mathrm{rel}^2/4$ per collision, and the heating rate of neutrons is equal to that of protons (equation 67). The neutron temperature $kT_\mathrm{n} = (2/3)\bar{E}_\mathrm{n}$ may be estimated by integrating the heating rate per neutron $d\bar{E}_\mathrm{n}/\mathrm{d}r \approx (m_\mathrm{p}c^2/2r)\beta_\mathrm{rel} \approx (m_\mathrm{p}c^2/2r)(r/R_\mathrm{np})^3$ from $r = 0$ to R_np. This gives a modest value $kT_\mathrm{n} \sim 100\,\mathrm{MeV}$. A more accurate calculation, which includes adiabatic cooling of neutrons, may give even lower T_n. We conclude that the mean relative energy of *n–n* collisions, $E_\mathrm{nn} = 3kT_\mathrm{n}$, is well below 700 MeV, so only a tail of the quasi-Maxwellian distribution will contribute to destruction of neutrons.

Therefore, most of n–n collisions at $r \sim R_{\rm np}$ are expected to be elastic, and a small fraction ζ of these collisions will convert neutrons to protons. The lifetime of a neutron at $r \sim R_{\rm np}$ is $\tau_{\rm n\to p} \approx \zeta^{-1}\,\xi^{-1}\tau_{\rm exp}$. An initially high neutron-to-proton ratio ξ will be reduced by conversion at decoupling if $\xi^{-1}\,\tau_{\rm n\to p} < \tau_{\rm exp}$, i.e. if the initial ξ exceeds $\zeta^{-1/2}$.

The exact ζ and the corresponding upper bound $\xi_{\rm max}$ may be found with detailed kinetic calculations of collisions. Such calculations are not attempted here, and we consider an optimistic range of $\xi < 10$ which might remain intact after decoupling. The case $\xi_0 = 4$ is chosen as a main example model.

3.7 Pair cascade initiated by π^0

Collisions between baryons near decoupling can produce neutral pions π^0 via reactions $p + p \to p + p + \pi^0$, $n + p \to d + \pi^0$ and $n + n \to n + n + \pi^0$. Decay of π^0 initiates a pair cascade in the outflow (DKK99a).

The inelastic p–p collisions are relatively rare at $\xi > 1$, especially when protons are cooled by Coulomb collisions with electrons. Reaction $n + p \to d + \pi^0$ has a maximum cross-section $\sim$0.1 of the elastic cross-section, and yields only $\sim 0.1\pi^0$ per proton at decoupling.

The cross-section of reaction $n + n \to n + n + \pi^0$ is $\sim$1/4 times smaller than cross-section of $n + n \to n + p + \pi^-$. (These reactions have the same cross-sections as the experimentally studied reactions $p + p \to p + p + \pi^0$ and $p + p \to p + n + \pi^+$, respectively.) Hence, the time-scale of π^0 production by a neutron is four times longer than $\tau_{\rm n\to p}$ which is in turn longer than $\tau_{\rm exp}$ (Section 3.6). This implies that up to $\sim 0.2\pi^0$ is produced per neutron at decoupling, or $\sim 0.2\xi \sim 1\,\pi^0$ per electron.

A typical produced π^0 has energy of a few hundred MeV. It immediately decays into two photons, and the high-energy photons are absorbed by the thermal radiation (DKK99a). As a result, a relativistic $e^\pm$ pair is created which upscatters thermal radiation, and the upscattered photons create a new generation of pairs. A maximum possible pair yield of the initiated cascade, $Y \approx 0.1$, would be achieved if the cascade were 'saturated', i.e. if the upscattered gamma-rays always got absorbed by softer photons (Svensson 1987). Thus maximum 10 per cent of the π^0 energy could possibly be converted into pair rest mass, which corresponds to $\sim 30e^\pm$ per injected π^0. The cascade is not, however, saturated: after a few generations, the upscattered gamma-rays are able to escape the thermal radiation (DKK99a). Therefore, a more realistic pair yield is a few per cent. It corresponds to roughly $10e^\pm$ injected per proton in the outflow. Most of these pairs annihilate soon after injection at $r \sim R_{\rm np}$.

The inelastic n–n collisions also happen at $r > R_{\rm np}$ with increasing time-scale $\propto n^{-1} \propto r^2$, and the pair creation remains significant until $r \sim 4R_{\rm np}$. The created pairs increase the opacity of the outflow and reduce the time-scale of Coulomb interactions between protons and electrons. In Section 3.8 this effect is neglected.

3.8 Numerical models

Figs 4 and 5 show two numerical models of neutron-loaded outflows with initial neutron-to-proton ratio $\xi_0 = 4$. The first model has $\eta = 300$ and the second model has $\eta = 3 \times 10^3$. In both cases, $\eta > \eta_*$ and the decoupling $\Gamma_{\rm p} > \Gamma_{\rm n}$ takes place. It is especially significant in the high-η model.

The evolution of Lorentz factors $\Gamma_{\rm n}$ and $\Gamma_{\rm p}$ has three stages: (i) acceleration of both components which ends with different saturated values of $\Gamma_{\rm n}$ and $\Gamma_{\rm p}$. Note that neutrons decouple earlier in the $\eta = 3 \times 10^3$ model and therefore have a smaller $\Gamma_{\rm n}$ compared to the $\eta = 300$ model. (ii) Coasting stage $\Gamma_{\rm n} = {\rm const}$ and $\Gamma_{\rm p} = {\rm const}$. (iii) Deceleration of the proton component by decaying neutrons. At about the same time the outflow begins to experience deceleration by an external medium. We do not study the

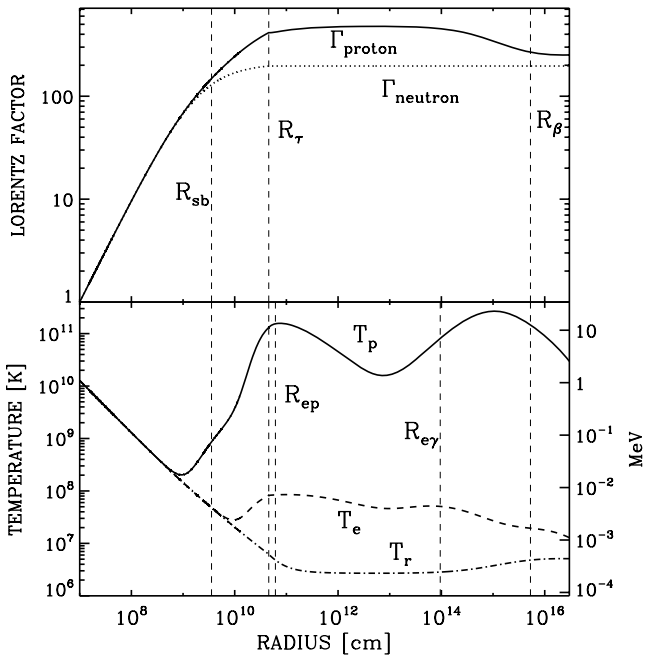

Figure 4. Evolution of a neutron-loaded outflow with $\xi_0 = 4$, $\eta = 300$, $L = 10^{52}\,{\rm erg\,s^{-1}}$ and $R_0 = 10^7$ cm. Upper panel: Lorentz factors of proton and neutron components (solid and dotted curves, respectively). Bottom panel: temperatures of protons (solid curve), electrons (dashed curve) and radiation (dash–dotted curve). Vertical dashed lines indicate characteristic radii $R_{\rm sb}$, R_τ, $R_{\rm ep}$, $R_{e\gamma}$ and R_β (see the text). The decoupling radius $R_{\rm np}$ is close to $R_{\rm sb}$.

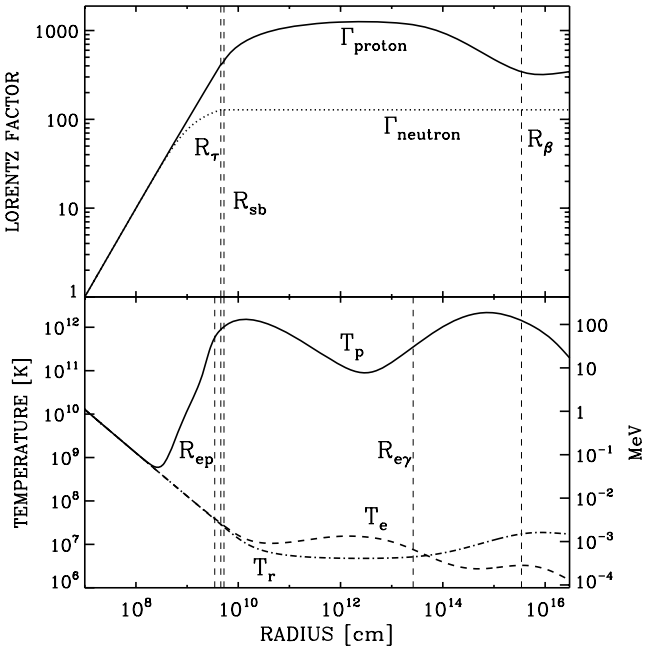

Figure 5. Same as Fig. 4 but for $\eta = 3 \times 10^3$.

external deceleration in the present paper and stop our calculations at $r = 3 \times 10^{16}$ cm.

The evolution of proton temperature $T_{\rm p}$ has an initial decline followed by two pronounced peaks. The first peak happens at the end of neutron acceleration. It is caused by the strong friction between the n and p components near the decoupling radius $R_{\rm np}$. The second peak accompanies the deceleration of protons at $r \lesssim R_\beta$ – it is caused by absorption of decayed neutrons by the proton outflow. The overall thermal evolution is markedly different from the neutron-free case and we describe it below in more detail.

At the beginning of outflow expansion, the thermal evolution is similar to the neutron-free case: all components are thermally coupled at a common temperature. The temperature is controlled by radiation (which strongly dominates heat capacity of the outflow) and decreases according to adiabatic law with $\hat{\gamma} = 4/3$.

The behaviour changes when the Lorentz factor $\Gamma_{\rm p} \approx \Gamma_{\rm n}$ reaches a value about 50. Then the proton temperature decouples from $T_{\rm e}$ and $T_{\rm r}$ and begins to grow. This is the result of the frictional heating and the quickly increasing relative velocity between n and p components. Only a fraction of the frictional heat is kept by baryons and a quasi-steady energy circulation is maintained in the accelerating outflow: radiation $\rightarrow$ relative kinetic energy of the n and p components $\rightarrow$ baryonic heat $\rightarrow$ electrons $\rightarrow$ radiation. The thermal balance of protons in this circulation controls $T_{\rm p}$, and $T_{\rm p}$ quickly grows as the outflow approaches the n–p decoupling radius.

After the decoupling radius, the n–p collisions become rare and the frictional heating extinguishes. On the other hand, the protons get thermally decoupled from electrons because of a long time-scale of Coulomb energy exchange. The subsequent decrease of $T_{\rm p}$ is mainly caused by adiabatic cooling.

Adiabatic cooling continues until the heating by β decay interferes the thermal evolution. The time-scale of adiabatic cooling in the proton frame is $r/c\Gamma_{\rm p}$ which is proportional to r during the coasting stage. By contrast, the time-scale of β decay is constant. Therefore, the heating of protons by decayed neutrons wins the adiabatic cooling at some point, and $T_{\rm p}$ begins to grow as $T_{\rm p} \propto r$. This growth continues until the outflow approaches R_β where most of the neutrons decay. The exponential extinction of neutrons implies that heating extinguishes at $r \sim R_\beta$. Then the outflow again cools adiabatically.

The two main effects of neutrons on the outflow–heating and deceleration of the proton component–are especially strong at high ξ_0 and high η. This is illustrated in Figs 6 and 7 which show models with $\xi_0 = 1$, 4, 10 and $\eta = 300$, 3×10^3. At high ξ_0 and/or η the proton density of the outflow is low and the n–p decoupling occurs early, leading to a large relative Lorentz factor $\Gamma_{\rm rel}$ between the n and p components. The large kinetic energy of the relative motion is then available for dissipation.

We also note that outflows with very high η and ξ_0 quickly become transparent and most of their energy is carried away by thermal radiation. This is illustrated by Fig. 8 which shows three components of the outflow luminosity: radiation, protons and neutrons. The radiation luminosity is given by $L_\gamma = 4\pi r^2 c \beta_{\rm p} \Gamma_{\rm p}^2 ((4/3) a T_{\rm r}^4)$ for $r < R_\tau$ and remains constant after R_τ. The kinetic luminosities of protons and neutrons are $L_{\rm p} = 4\pi r^2 c \beta_{\rm p} \Gamma_{\rm p}^2 \rho_{\rm p} c^2$ and $L_{\rm n} = 4\pi r^2 c \beta_{\rm n} \Gamma_{\rm n}^2 \rho_{\rm n} c^2$. The sum of three contributions remains constant and equals the total luminosity $L = 10^{52}$ erg s^{-1}. One can see that the outflow with $\xi_0 = 4$ and $\eta = 300$ emits about 30 per cent of its energy at the transparency radius, and the outflow with $\eta = 3 \times 10^3$–more than 90 per cent.

All numerical models shown in Figs 4–8 assumed that the outflow starts to accelerate at radius $R_0 = 10^7$ cm. This is a reasonable assumption if the outflow forms near a stellar-mass compact object and expands either spherically or conically with a constant opening angle $\theta_j > 1/\Gamma_{\rm p}$. It is likely, however, that the free conical expansion is preceded by a collimation stage (as envisioned by, e.g. collapsar model of MacFadyen & Woosley 1999). During the collimation stage $\theta_j(r)$ decreases and the jet is hardly accelerated inside the

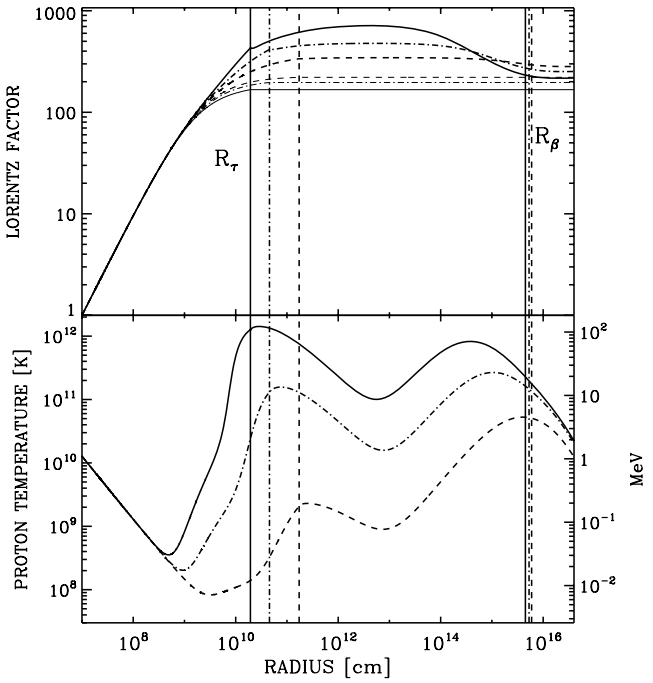

Figure 6. Evolution of outflows with the same parameters as in Fig. 4 but with different $\xi_0 = 1$ (dashed curves) and $\xi_0 = 10$ (solid curves). The model with $\xi_0 = 4$ from Fig. 4 is shown by the dash–dotted curves. Upper panel: Lorentz factors of proton and neutron components. Lower panel: proton temperature.

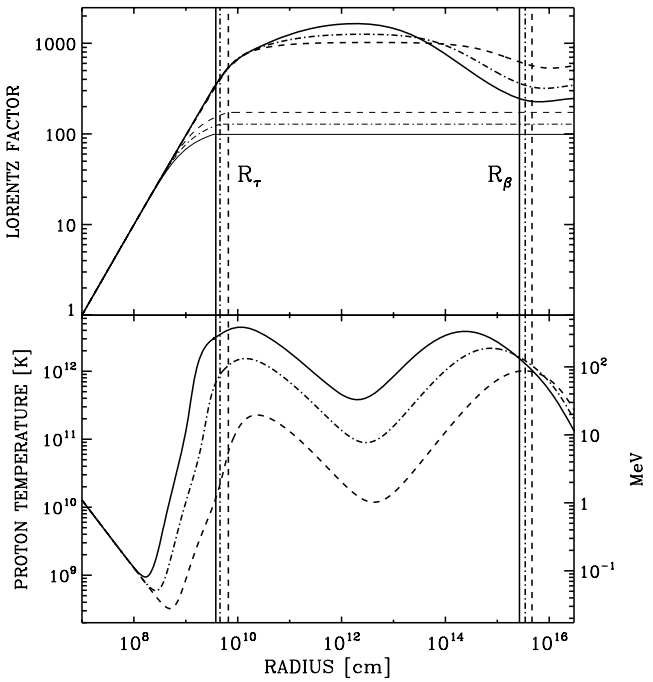

Figure 7. Same as Fig. 6 but for outflows with $\eta = 3 \times 10^3$.

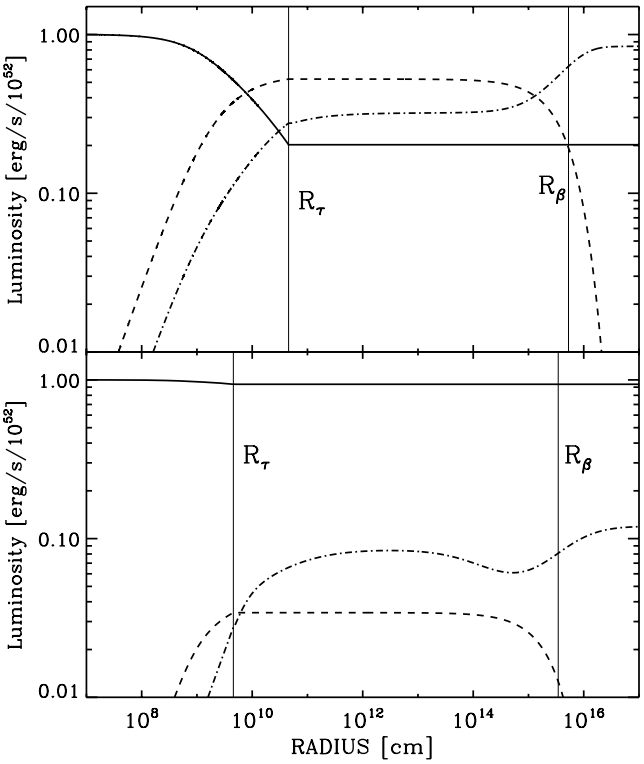

Figure 8. Contributions to the energy outflow rate from radiation (solid curve), protons (dash–dotted curve) and neutrons (dashed curve). The sum of the three luminosities $L_\gamma + L_\mathrm{p} + L_\mathrm{n}$ is constant and equal to $L = 10^{52}$ erg s^{-1}. The upper panel corresponds to the model shown in Fig. 4, and the lower panel to the model shown in Fig. 5.

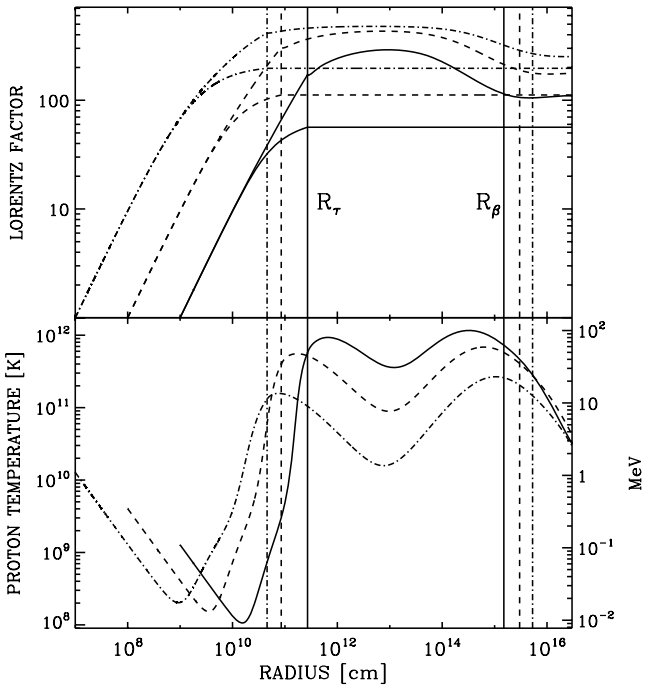

Figure 9. Evolution of outflows with the same parameters as in Fig. 4 but with different $R_0 = 10^8$ cm (dashed curves) and $R_0 = 10^9$ cm (solid curves). The model with $R_0 = 10^7$ cm from Fig. 4 is shown by the dash–dotted curves. Upper panel: Lorentz factors of proton and neutron components. Lower panel: proton temperature.

progenitor star until it reaches the break-out radius R_0 and starts free expansion with $\theta_j(r) = \text{const}$ and acceleration $\Gamma_\mathrm{p} \propto r$. Then our spherical/conical model applies with a large effective R_0.

To see how the outflow dynamics is changed by collimation, we have calculated numerical models with $R_0 = 10^7, 10^8, 10^9$ cm. The results are shown in Fig. 9. When R_0 is large, a given Lorentz factor is reached at a smaller density of the outflow. As a result, neutrons decouple at a smaller Lorentz factor Γ_n and the outflow develops a larger Γ_rel, leading to strong heating. This trend is observed in Fig. 9. Outflows with large R_0 also have smaller Γ_p and most of their energy is carried away by thermal radiation released at the transparency radius.

We also note that explosions with large R_0 have larger decoupling radii R_np and R_τ, and a smaller decay radius R_β. Therefore, the two peaks of frictional and β-decay heating are closer to each other, and the stage of adiabatic cooling between them shortens. At even larger $R_0 \gtrsim 10^{10}$ the two peaks would overlap.

4 DISCUSSION

In this paper, we developed the theory of relativistic neutron-loaded outflows. The presence a neutron component significantly affects the early dynamics of GRB explosions. In particular, the plasma temperature is increased by many orders of magnitude, and this heating can compete with other heating mechanisms such as internal shocks or dissipation of magnetic fields in the outflow.

The effects of neutrons are pronounced in outflows with $\eta > \eta_*$ given by equation (55), whose typical value is several hundred. Then neutrons and protons develop a substantial relative Lorentz factor which leads to strong heating and momentum exchange when neutrons decay. We also note that neutron-rich outflows with very high $\eta \gg \eta_*$ lose most of their energy at the photosphere: their thermal radiation carries most of the energy at the moment of transparency. Therefore, the neutron effects may be especially strong in GRBs with a significant thermal component in the radiation spectrum (a number of such GRBs have been identified recently, see e.g. Ghirlanda, Celotti & Ghisellini 2003; Ryde 2004).

The calculations in this paper focused on the simplest model of a uniform hydrodynamic outflow with weak magnetic fields. We did not consider, for instance, internal shocks (e.g. Rees & Mészáros 1994) and possible pair creation by non-thermal gamma-rays generated in the outflow. Pair creation may extend the optically thick stage of expansion, and the trapped radiation may convert its energy more efficiently into bulk kinetic energy of the plasma. A large-scale magnetic field may gradually collimate the outflow so that the conical geometry of expansion does not apply (Vlahakis, Peng & Königl 2003).

The β decay is likely to affect the development of internal shocks in the outflow. The shocks are caused by a non-uniform profile of the Lorentz factor, and the drag effect of decayed neutrons tends to smoothen this profile. The fastest portions of the outflow are more effectively decelerated and the initial contrast of Lorentz factors may be substantially reduced already at $r \sim 10^{14}$ cm. This effect constrains the dissipation efficiency of the shocks, which is sensitive to the contrast of Lorentz factors (see fig. 3 in Beloborodov 2000). In addition, the high temperature of the outflow heated by β decay may prevent development of the shocks. We defer a detailed study of these effects to a future work.

The impact of neutrons on the prompt burst and its afterglow provides a unique opportunity to link the observed emission with

physical conditions in the central engine of the explosion. The very presence of neutrons is a signature of an extremely hot and dense engine. Observable effects of neutrons may shed light on the mechanism of GRB trigger.

ACKNOWLEDGMENTS

AMB was supported by NASA Grant NAG5-13382 and the Alfred P. Sloan Fellowship. This research was supported in part by the National Science Foundation under Grant No. PHY99-07949.

REFERENCES

Bahcall J. N., Mészáros P., 2000, Phys. Rev. Lett., 85, 1362
Beloborodov A. M., 2000, ApJ, 539, L25
Beloborodov A. M., 2002, ApJ, 565, 808
Beloborodov A. M., 2003a, ApJ, 585, L19
Beloborodov A. M., 2003b, ApJ, 588, 931 (B03b)
Daum M. et al., 2002, Eur. Phys. J. C, 23, 43
Derishev V. K., Kocharovsky V. V., Kocharovsky V., Vl, 1999a, ApJ, 521, 640 (DKK99a)
Derishev V. K., Kocharovsky V. V., Kocharovsky V., Vl, 1999b, A&A, 345, L51
Fuller G. M., Pruet J., Abazajian K., 2000, Phys. Rev. Lett., 85, 2673
Ghirlanda G., Celotti A., Ghisellini G., 2003, A&A, 406, 879
Lemoine M., 2002, A&A, 390, L31
MacFadyen A. I., Woosley S. E., 1999, ApJ, 524, 262
Mészáros P., Rees M. J., 2000a, ApJ, 541, L5
Mészáros P., Rees M. J., 2000b, ApJ, 530, 292
Misner C. W., Thorne K. S., Wheeler J. A., 1973, Gravitation. Freeman & Co., San Francisco
Piran T., 1999, Phys. Rep., 314, 575
Pruet J., Guiles S., Fuller G. M., 2002, ApJ, 580, 368
Rees M. J., Mészáros P., 1994, ApJ, 430, 93
Ryde F., 2004, ApJ, 614, 827
Shimizu F., Kubota Y., Koiso H., Sai F., Sakamoto S., Yamamoto S. S., 1982, Nucl. Phys. A, 386, 571
Stepney S., 1983, MNRAS, 202, 467
Svensson R., 1987, MNRAS, 227, 403
Vlahakis N., Peng F., Königl A., 2003, ApJ, 594, L23

This paper has been typeset from a TEX/LATEX file prepared by the author.